

Keto-enol tautomerism of (E)-2-[(3,4-dimethylphenylimino)methyl]-4-nitrophenol: Synthesis, X-ray, FT-IR, UV–Vis, NMR and quantum chemical characterizations

Arzu Özak Yıldırım ^{a,*}, M. Hakkı Yıldırım ^b, Çiğdem Albayrak Kaşaş ^c

^a Faculty of Arts and Science, Giresun University, Turkey

^b Dereli Vocational School, Giresun University, Turkey

^c Samsun Vocational School, Ondokuz Mayıs University, Turkey



ARTICLE INFO

Article history:

Received 16 May 2016

Received in revised form

28 July 2016

Accepted 30 July 2016

Available online 31 July 2016

Keywords:

Schiff base

NLO

X-ray

GTO

STO

Tautomerism

ABSTRACT

(E)-2-((3,4-dimethylphenylimino)methyl)-4-nitrophenol, which is a new Schiff base compound, was synthesized and characterized by experimental and computational methods. Molecular geometry, harmonic oscillator model of aromaticity (HOMA) indices, intra- and inter-molecular interactions in the crystal structure were determined by using single crystal X-ray diffraction technique. The optimized structures, which are obtained by Gaussian and Slater type orbitals, were compared to experimental structures to determine how much correlation is found between the experimental and the calculated properties. Intramolecular and hyperconjugative interactions of bonds have been found by Natural Bond Orbital analysis. The experimental infrared spectrum of the compound has been analyzed in detail by the calculated infrared spectra and Potential Energy Distribution analysis. To find out about the correlation between the solvent polarity and the enol-keto equilibrium, experimental UV–Visible spectra of the compound were obtained in benzene, CHCl₃, EtOH and DMSO solvents. In these solvents, the UV–Vis spectra and relaxed potential energy surface scan (PES) calculations have been performed to get more insight into the equilibrium dynamics. Solvent effects in UV–Vis and PES calculations have been taken into account by using Polarizable Continuum Modelling method. ¹H and ¹³C NMR spectra of the compound (in DMSO) were analyzed. The computational study of nonlinear optical properties shows that the compound can be used for the development of nonlinear optical materials.

© 2016 Elsevier B.V. All rights reserved.

1. Introduction

In recent years, synthesis and characterizations of the Schiff base compounds and their metal complexes have attracted the attention of researchers [1–10]. Their potential applications can be found in chemistry [11–14], pharmaceutical and biological fields [15–17]. Schiff bases can display photochromic and thermochromic properties, depending on the prototropic tautomerism, the molecular geometry and the crystal packing [18,19]. The migration of a proton between the two stable form of the molecule has been defined as the prototropic tautomerism by Lapworth and Hann [20]. In spite of the relatively only a small fraction of the molecules has this feature, the prototropic tautomerism has received the

attention of researchers. In Schiff bases, the prototropic tautomerism emerges from the transformation of the enol tautomeric form [21] to keto tautomeric form [22] and vice versa. In addition to the effects of the media, the electron donating and withdrawing substituents affect the tautomeric form of the molecule [23].

In the current study, a new Schiff base, (E)-2-[(3,4-dimethylphenylimino)methyl]-4-nitrophenol, has been firstly synthesized, the structural and electronic properties characterized by using spectroscopic techniques and the computational methods. Molecular structure and intermolecular interactions have been found by using single crystal X-ray diffraction techniques. Its spectral characterizations have been carried out by experimental Fourier transform infrared, proton and carbon NMR, UV–Visible spectroscopy and computational (DFT and TD-DFT) methods. Also, the geometry optimization and infrared spectrum calculations were performed by using Slater type orbitals (STO) in Amsterdam Density Functional (ADF) software. The tautomeric equilibrium of

* Corresponding author.

E-mail address: arzu.ozek.yildirim@giresun.edu.tr (A. Özak Yıldırım).

the compound between the enol, keto and transition state (TS) forms have been investigated in the vacuum and solvent media. In addition, nonlinear optical (NLO) properties and Natural Bond Orbital (NBO) analysis of the compound have been studied by DFT methods.

2. Material and methods

2.1. Synthesis

(E)-2-[(3,4-dimethylphenylimino)methyl]-4-nitrophenol was prepared by refluxing a mixture of 2-hydroxy-5-nitrobenzaldehyde (0.5 g, 3 mmol) in 20 ml ethanol and 3,4-dimethylaniline (0.36 g, 3 mmol) in 20 ml ethanol for 1 h. The pure single crystals of the compound were acquired by slow evaporation of ethanol solution (yield: 86%, m.p. 451–453 K).

2.2. Spectroscopic measurements

Fourier transform infrared spectral data was collected in the 4000–400 cm^{-1} region with a Bruker Vertex 80 V spectrometer using KBr pellet technique. UV–Visible spectra were measured within 200–800 nm range in benzene, chloroform, ethanol and DMSO solvents on a Thermo Scientific Evolution Array spectrometer. The ^1H and ^{13}C NMR spectral data were obtained in DMSO solution on a Bruker AVANCE III 400 MHz spectrometer using TMS as an internal reference.

2.3. Single crystal structure determination

Data collection were performed with a STOE IPDS II diffractometer by using MoK α radiation at 296 K. The crystal structure solution was found by using SHELXS [24] and structure refined with SHELXL [24] in WinGX software [25]. Position of H1 atom (hydroxyl hydrogen) was found from a difference Fourier map and the other H atoms were located geometrically. Molecular drawing was prepared with ORTEP-3 for Windows [26] and the crystal packing figure was drawn by PLUTON [27] software. The details of crystal structure solution and the refinement were given in Table S1 (Supplementary material). The crystallographic information file of the compound can be obtained from The Cambridge Crystallographic Data Centre (CCDC 1043761) via www.ccdc.cam.ac.uk/structures.

2.4. Computational methods

Gaussian type orbital calculations (GTO) were performed by using Gaussian 09W [28] software at the DFT/B3LYP level of theory [29] with 6–311++G (d,p) basis set. The molecular geometry obtained from X-ray diffraction was selected as an initial geometry of the enol structure and this geometry has been fully optimized with Berny optimization algorithm [30] in Gaussian 09W. The changes in the molecular structure during the proton transfer process have been acquired by doing relaxed potential energy surface (PES) scan calculations in the vacuum and solvent media along the O–H···N path (moving H atom from O to N). The initial geometries of TS and keto tautomer were obtained from PES calculation in vacuum. The global maximum on PES coordinate corresponds to TS, while the local minimum represents keto tautomer. Berny transition state optimization technique was used for transition state optimization. Frequency calculation of the optimized TS structure gave one negative value which is correspond to proton transfer coordinate. GTO and STO type infrared spectra calculations of the compound were performed on the optimized enol structure in the vacuum. The frequencies were scaled by 0.9688 [31] for GTO and 0.9648 [32]

for STO. Potential energy distributions and assignments of the scaled GTO frequencies were calculated by using VEDA4 software [33]. Theoretical UV–Vis. spectra of the enol and keto structures were obtained with the TD-DFT/B3LYP method [34–37]. Solvent effects in the potential energy surface scan calculations, enol/keto structure optimizations and theoretical UV–Vis. spectra calculations were modelled by using Polarizable Continuum Model (PCM) [38,39]. All the Slater type orbital (STO) calculations were performed by using ADF 2009.01 [40–42] software package. Geometry optimization and infrared calculation were carried out using DFT/B3LYP methods, with the TZP basis sets.

3. Results and discussion

3.1. Molecular and crystal structure

The titled compound crystallizes in the centrosymmetric *P*-1 space group. Molecular structure of the compound with atom labelling scheme is given in Fig. 1. The all geometric parameters with corresponding calculated values have been presented in Table S2.

X-ray crystallography analysis of the compound reveals that the C2–O1 (1.328 (4) Å) bond length indicates a single-bond character, whereas the C7–N1 (1.290 (4) Å) bond length indicates a double-bond character. Hence, the prototropic hydrogen atom (H1) is located on atom O1, thus showing a preference for the phenol–imine tautomer in the solid state. Bond lengths of the nitro group, which are N2–O2 and N2–O3, are found to be 1.227 (4) and 1.227 (3). The other structural parameters are in harmony with related Schiff base compounds [43,44]. According to Mavridis et al. [45], thermochromic and photochromic properties are associated with the molecular planarity in Schiff bases. The dihedral angle between C1/C6 and C8/C13 rings showing the planarity of the title molecule is 1.205 (2) $^\circ$ and this planarity may lead to a thermochromic feature.

The optimized geometries of the compound obtained by using the GTO and STO were in the harmony with the XRD geometry. The root mean square errors (RMSE) in bond lengths have been calculated as 0.091 Å for XRD/GTO comparison and 0.089 Å for XRD/STO comparison while the RMSE's of bond angles have been calculated as 1.54 $^\circ$ and 1.48 $^\circ$, respectively. For the bond lengths, the biggest deviations occur at C7–H7 and C9–H9 bonds with the difference being 0.165 Å, 0.155 Å for GTO and 0.162 Å, 0.151 Å for STO, respectively. C2–O1–H1 bond angle has the greatest differences for the bond angle with 5.6 $^\circ$ for GTO and 6.1 $^\circ$ for STO. The largest deviations between the experimental and calculated values are observed in the bond length and angle involved in hydrogen bonds. Besides that, to visualize the results of RMS calculations, a superimposition of the experimental and calculated structures is given in

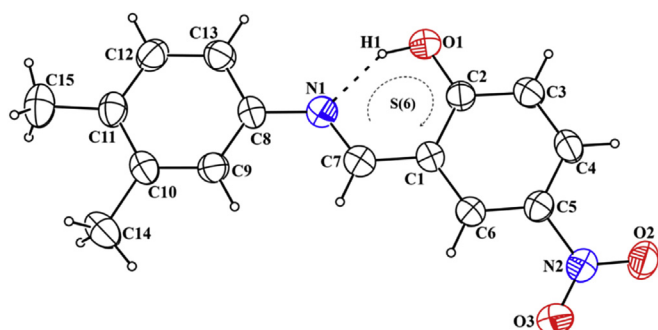


Fig. 1. Ortep-III molecular drawing of the title compound.

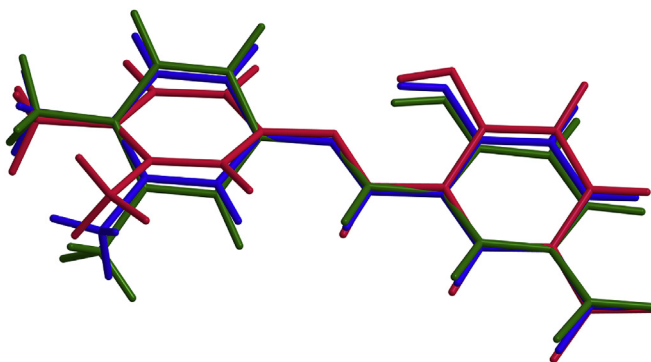


Fig. 2. Superimpositions of the experimental (blue), GTO (red) and STO (green) structures of the title compound. (For interpretation of the references to colour in this figure legend, the reader is referred to the web version of this article.)

Fig. 2. Deviations of dihedral angle between the aromatic rings can be explained by considering the intermolecular interactions with the adjacent molecules are absent in the theoretical calculations, whereas the experimental result corresponds to interacting molecules in the crystal structure [46].

As in most of *o*-hydroxysalicylidene systems [43,47], a resonance assisted hydrogen bond (RAHB) between the Schiff base linkage and hydroxyl group has been found in crystal structure of the title compound. In this hydrogen bond, the O1···N1 distance is 2.558 Å, which is shorter than the sum of the van der Waals' radii for N and O atoms [48]. This strong hydrogen bond (O1—H1···N1) generates an S (6) ring motif (Fig. 1) in the molecular structure. Among the intermolecular interactions of the compound, C7—H7···O3ⁱ (i: -x, 1-y, 1-z) hydrogen bonds are the strongest interaction and they generate centrosymmetric $R_2^2(14)$ dimers. These dimers are interconnected by C15—H15B ... Cg1ⁱⁱ (Cg1 is the centroid of C8—C13 ring, ii: 2-x, 1-y, -z) C—H···π interactions and the resulting partial packing diagram is given in Fig. 3. The geometric details of the intermolecular interactions are given in Table S3.

3.2. The intramolecular proton transfer process

In order to examine the effects of intramolecular proton transfer on the molecular geometry and energy, potential energy surface (PES) calculations have been performed for the proton transfer coordinate in vacuum and various solvents. O1—H1 bond has been selected as a scan coordinate and it has been varied from 0.9 to 1.7 Å with the step size of 0.05 Å. Obtained scan graphics of the relative energy against the bond length are given in Fig. 4. Relative energies have been calculated by using the energy of stable keto tautomer in

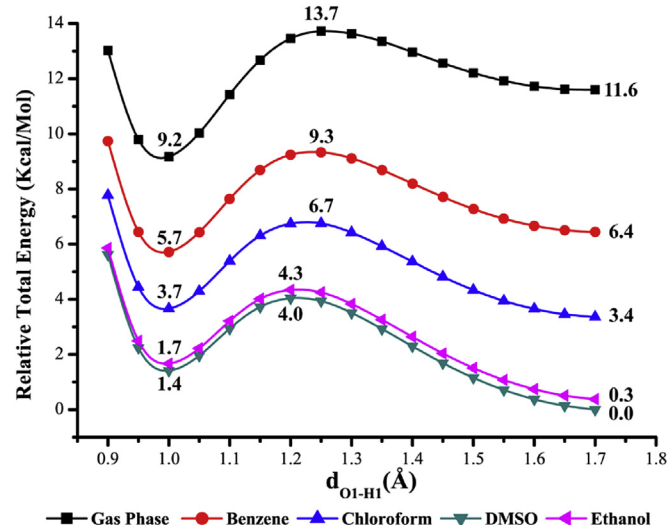


Fig. 4. The graph of the relative energy against the O1—H1 bond distance in PES scan process.

DMSO as a reference energy. It is found that the energy of the enol form is less than the keto form in vacuum and benzene while the keto form is more stable than the enol form in CHCl₃, ethanol and DMSO solvents. Also, the barrier between enol and keto form decreases (changing from 2.4 kcal/mol to -1.4 kcal/mol) with the increasing solvent polarity. Consequently, enol-keto tautomerization in a polar solvent may take place more easily compared to an apolar solvent.

Delocalization of π electrons in a ring is easily affected by proton transfer process. Thus, HOMA indices of the rings can be used as a descriptor of prototropic tautomerism. Geometry based local HOMA indices of a ring is calculated by using the following equation [49,50]:

$$HOMA = 1 - \frac{1}{n} \sum_{i=1}^n \alpha_i (R_i - R_{i,opt})^2 \quad (1)$$

where n is the number of bonds in the ring, α_i (1/Å²) is a normalization constant (257.7 for C—C, 93.52 for C—N and 157.38 for C—O bonds), R_i is the experimental or calculated bond length and $R_{i,opt}$ optimized bond length is equal to 1.388 Å for C—C, 1.334 Å for C—N and 1.265 Å for C—O bonds. For the aromatic ring, HOMA value is in the range of 0.90–0.99 while HOMA value of the non-aromatic ring is in the range of 0.50–0.80 [51,52]. The calculated HOMA indices (using XRD bond lengths) for the C8—C13 (A), C1—C6 (B), and quasi (C) rings are 0.961, 0.898 and 0.606 respectively. From these results,

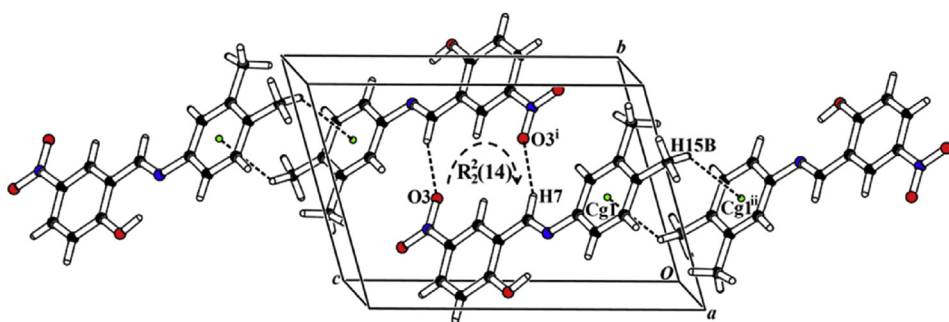


Fig. 3. A partial packing diagram for the title compound, intermolecular interactions shown as dashed lines. Cg1 is the centroid of C8—C13 ring. [Symmetry codes: (i) -x, 1-y, 1-z; (ii) 2-x, 1-y, -z].

the RAHB in the molecule decreases the aromaticity of B ring, while increases the aromaticity of C ring. Also, the effects of the intramolecular proton transfer on the molecular geometry can be monitored by observing the changes in HOMA indexes.

During the proton transfer process, the HOMA indexes of A, B and C rings were calculated at each step. As can be seen from Fig. 5, HOMA value of B ring decreases with the scan coordinate going from 0.9 to 1.7 Å while HOMA value of quasi C ring first increases up to 0.61 at 1.3 Å (transition state) and then decreases to a final value of 0.52. When considering these results, during the proton transfer process, aromaticity of the B ring is transferred to into C quasi ring, indicating the π -electron coupling for the molecule [53]. It can be seen from Fig. 5, HOMA values of A ring do not change with the scan coordinate and the ring preserves its aromaticity during the proton transfer process as found in the previous studies [47,54].

3.3. Experimental and calculated infrared spectra

The experimental and the calculated (by GTO and STO) infrared vibrations with the Potential Energy Distributions (PED) assignments are listed in Table 1, comparatively.

Vibrational frequencies have been assigned using PED values that were calculated with the aid of VEDA4 program [33]. The calculated frequencies were scaled by 0.9687, which is scaling factor for B3LYP [31]. The experimental (in solid state) and calculated (in vacuum) FT-IR spectrum of the compound are shown in Fig. 6.

Broad absorption band in the 3000–1600 cm^{−1} is due to presence of strong intramolecular hydrogen bonding between the N and O atom. This OH stretching vibration was calculated at 2993 cm^{−1} (GTO) and 2966 cm^{−1} (STO).

Stretching vibrations of a methine (aliphatic) group usually are found at below 3000 cm^{−1} regions [55]. The C7–H7 stretching vibration was located at 2918 cm^{−1} while calculated at 2955 cm^{−1}. The aromatic C–H stretching vibrations were observed in the region 3101–3039 cm^{−1} experimentally and calculated in the region 3121–3063 cm^{−1} [56]. The aromatic C–H in-plane bending vibrations were found in the region 1488–1184 cm^{−1}, while calculated results are in the range of 1479–1192 cm^{−1}. The peak observed at 906 cm^{−1} is attributed to the aromatic C–H out-of-plane bending vibration. This mode was calculated to be 899 cm^{−1}.

The asymmetric and symmetric stretching vibrations of methyl

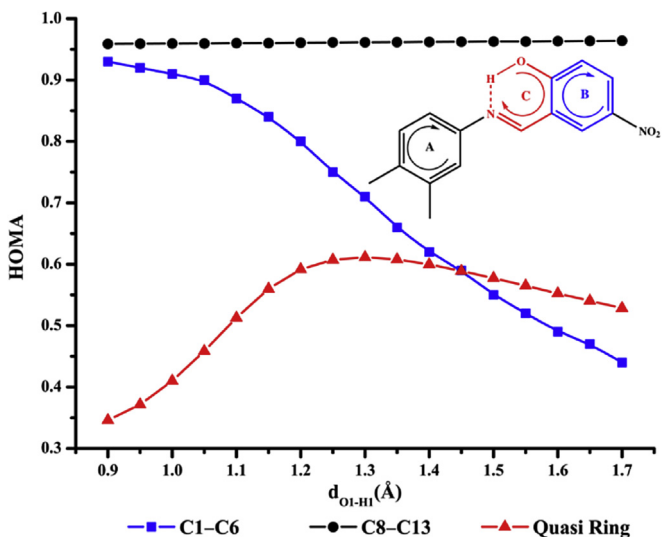


Fig. 5. The graph of HOMA indexes against the O1–H1 bond distance in PES scan process.

group in aromatic compounds are expected in the range 3000–2925 cm^{−1} and 2940–2905 cm^{−1}, respectively [57]. The bands at 3011 and 2942 cm^{−1} in the experimental FT-IR spectra are attributed to the asymmetric and symmetric methyl stretching vibrations, while these modes have been calculated at 3009, 2971 and 2966 cm^{−1}, respectively. In addition, in plane bending and out of plane bending vibrations of CH₃ groups were observed at 1451 cm^{−1} and 1373 cm^{−1} experimentally, and calculated at 1449, 1447, 1445 cm^{−1} and 1378, 1368 cm^{−1}, respectively.

As found in XRD study, C7=N1 is double bond character. Considering this result, the sharp absorption band at 1619 cm^{−1} is attributed to C7=N1 stretching vibration. This vibration band has been calculated at 1618 cm^{−1} and 1616 cm^{−1} by GTO and STO calculations.

In the aromatic nitro compounds, asymmetric and symmetric stretching vibrations of the nitro group have strong absorptions bands in the region 1570–1485 cm^{−1} [58] and 1370–1320 cm^{−1}, respectively [59]. Corresponding vibrations of the nitro group in the title compound are observed at 1523 cm^{−1} and 1330 cm^{−1}, respectively. The GTO and STO type frequency calculations show that the nitro group asymmetric stretching vibrations are at 1532 cm^{−1}, 1527 cm^{−1} and symmetric stretching vibrations are at 1314 cm^{−1}, 1309 cm^{−1}, respectively.

The carbon–carbon stretching vibrations of aromatic compounds are expected to appear as a strong band in the region of 1650–1200 cm^{−1} [56]. Hence, the peaks in the region 1598–1381 cm^{−1} were attributed to the C–C aromatic stretching vibrations and calculated in the region 1611–1324 cm^{−1}.

3.4. Electronic spectra

As mentioned in section 3.2., the potential energy barrier between the enol and keto form varies with the solvent polarity. Therefore, one would expect the keto form more dominant than the enol form in polar solvent. For this reason, UV–Visible spectra of the compound were measured within 200–800 nm range in benzene, chloroform, ethanol and DMSO solvents. In addition, theoretical UV–Vis. spectra of the enol and keto structures were obtained by TD-DFT calculations with PCM solvent modelling method in the mentioned solvents. The calculated spectra were explained by means of the Frontier Molecular Orbitals (FMOs) with the aid of GaussSum software [60] and a comparative table of the experimental and the calculated absorbance values with their FMO assignments are given in Table S4. The experimental and the calculated spectra were given in Fig. S1.

In the UV–Visible spectrum of an o-hydroxy Schiff base, two maxima can be seen in connection with the tautomeric form of the Schiff base. A maximum less than 400 nm implies that an enol form, while a second maximum greater than 400 nm indicates that a keto form [61,62]. There are three maxima in the experimental spectra, except for benzene. The experimental maximum at about 312 nm corresponds to HOMO-1 → LUMO transition for the calculated spectra in benzene, while this maximum is formed by H-2 → L transition for the calculated spectra in the other solvents. The calculated transition between the HOMO and LUMO+1 in the all solvents gives a maximum at about 345 nm in the experimental spectra. These maxima can be attributed to the $\pi \rightarrow \pi^*$ transitions of –CH=N– group [61]. n → π^* transitions of the –C=O group in keto form are found at 443 nm in CHCl₃, 434 nm in ethanol, 426 nm in DMSO and they are shifted to shorter wavelengths (blue shift) with increasing solvent polarity. These maxima were calculated at 428 nm in CHCl₃, 425 nm in ethanol, 426 nm in DMSO and they are related to the HOMO → LUMO transitions of the keto structure. Also, these transitions indicate that the keto structure is found in the solvent media, as can be seen in Fig. S1, the keto/enol ratio increases

Table 1

Experimental and calculated infrared vibrations of the title compound with the PED assignments.

Experimental	GTO	STO	Assignment (%PED ^a)
3101	3121	3115	$\nu(\text{CH}) \text{R2}$ (92)
	3104	3099	$\nu(\text{CH}) \text{R2}$ (98)
	3099	3091	$\nu(\text{CH}) \text{R2}$ (91)
3071	3089	3081	$\nu(\text{CH}) \text{R1}$ (89)+ $\nu(\text{CH}) \text{R1}$ (11)
3056	3067	3063	$\nu(\text{CH}) \text{R1}$ (91)
3039	3064	3058	$\nu(\text{CH}) \text{R1}$ (81)+ $\nu(\text{CH}) \text{R1}$ (10)
3011	3009	3001	$\nu_{\text{as}}(\text{C}_\text{methyl}\text{H})$ (54)+ $\nu_{\text{as}}(\text{C}_\text{methyl}\text{H})$ (30)
	2993	2966	$\nu(\text{OH})$ (93)
2970	2971	2960	$\nu_s(\text{C}_\text{methyl}\text{H})$ (48)+ $\nu_s(\text{C}_\text{methyl}\text{H})$ (47)
	2966		$\nu_s(\text{C}_\text{methyl}\text{H})$ (48)+ $\nu_s(\text{C}_\text{methyl}\text{H})$ (48)
2942	2955	2933	$\nu(\text{C}_\text{methine}\text{H})$ (94)
2918	2927	2930	$\nu_s(\text{C}_\text{methyl}\text{H})$ (42)+ $\nu_s(\text{C}_\text{methyl}\text{H})$ (41)+ $\nu_s(\text{C}_\text{methyl}\text{H})$ (16)
2885	2924	2921	$\nu_s(\text{C}_\text{methyl}\text{H})$ (43)+ $\nu_s(\text{C}_\text{methyl}\text{H})$ (42)+ $\nu_s(\text{C}_\text{methyl}\text{H})$ (14)
1619	1618	1616	$\nu(\text{C}=\text{N})$ (46)
1598	1612	1608	$\nu(\text{CC}) \text{R2}$ (20)+ $\delta(\text{COH})$ (10)
1578	1583	1578	$\nu(\text{CC}) \text{R1}$ (18)+ $\nu(\text{CC}) \text{R}$ (14)
	1563	1560	$\nu(\text{CC}) \text{R2}$ (10)+ $\nu(\text{CC}) \text{R2}$ (11)+ $\delta(\text{COH})$ (10)
	1554	1549	$\nu(\text{CC}) \text{R1}$ (30)+ $\nu(\text{CC}) \text{R1}$ (11)
1523	1532	1527	$\nu_{\text{as}}(\text{NO}_2)$ (66)+ $\delta(\text{COH})$ (15)
1488	1480	1479	$\delta(\text{HCC}) \text{R1}$ (15)+ $\delta(\text{HCC}) \text{R1}$ (14)+ $\delta(\text{CCC}) \text{R1}$ (11)
1476	1470	1468	$\nu(\text{CC}) \text{R2}$ (12)+ $\delta(\text{COH})$ (21)+ $\delta(\text{HCC}) \text{R2}$ (13)
1451	1450	1448	$\alpha(\text{HC}_\text{methyl}\text{H})$ (11)+ $\alpha(\text{HC}_\text{methyl}\text{H})$ (17)+ $\alpha(\text{HC}_\text{methyl}\text{H})$ (30)
	1447	1446	$\alpha(\text{HC}_\text{methyl}\text{H})$ (23)+ $\alpha(\text{HC}_\text{methyl}\text{H})$ (30)
	1445	1445	$\alpha(\text{HC}_\text{methyl}\text{H})$ (19)+ $\alpha(\text{HC}_\text{methyl}\text{H})$ (17)+ $\alpha(\text{HC}_\text{methyl}\text{H})$ (12)+ $\alpha(\text{HC}_\text{methyl}\text{H})$ (28)
	1444	1441	$\nu(\text{OC})$ (10)+ $\nu(\text{CC}) \text{R2}$ (11)
	1433	1432	$\alpha(\text{HC}_\text{methyl}\text{H})$ (21)+ $\alpha(\text{HC}_\text{methyl}\text{H})$ (20)+ $\alpha(\text{HC}_\text{methyl}\text{H})$ (19)+ $\alpha(\text{HC}_\text{methyl}\text{H})$ (19)
	1400	1395	$\nu(\text{CC}) \text{R2}$ (26)+ $\nu(\text{CC}) \text{R2}$ (22)+ $\delta(\text{COH})$ (15)
1381	1390	1389	$\nu(\text{CC}) \text{R1}$ (14)+ $\nu(\text{CC}) \text{R1}$ (20)+ $\delta(\text{HCC}) \text{R1}$ (16)
1373	1378	1381	$\gamma(\text{CH}_3)$ (10)+ $\gamma(\text{CH}_3)$ (10)+ $\gamma(\text{CH}_3)$ (24)+ $\gamma(\text{CH}_3)$ (12)+ $\gamma(\text{CH}_3)$ (13)+ $\gamma(\text{CH}_3)$ (23)
	1368	1370	$\gamma(\text{CH}_3)$ (10)+ $\gamma(\text{CH}_3)$ (10)+ $\gamma(\text{CH}_3)$ (24)+ $\gamma(\text{CH}_3)$ (12)+ $\gamma(\text{CH}_3)$ (13)+ $\gamma(\text{CH}_3)$ (23)
1359	1339	1335	$\delta(\text{HC}=\text{N})$ (53)
	1325	1318	$\nu(\text{CC}) \text{R2}$ (23)+ $\nu(\text{CC}) \text{R2}$ (16)
1330	1314	1309	$\nu_s(\text{NO}_2)$ (60)
1291	1286	1280	$\nu(\text{CO})$ (41)+ $\delta(\text{HCC}) \text{R2}$ (17)
	1280	1276	$\delta(\text{CC}) \text{R1}$ (10)+ $\delta(\text{CC}) \text{R1}$ (24)+ $\delta(\text{CC}) \text{R1}$ (18)
	1266	1263	$\delta(\text{CC}) \text{R1}$ (10)+ $\delta(\text{HCC}) \text{R1}$ (25)+ $\delta(\text{HCC}) \text{R1}$ (23)
1232	1229	1226	$\nu(\text{C}=\text{N})$ (13)
1197	1216	1214	$\delta(\text{HCC}) \text{R2}$ (16)+ $\delta(\text{HCC}) \text{R2}$ (28)
1184	1192	1191	$\delta(\text{CC}) \text{R2}$ (10)+ $\nu(\text{C-C}_\text{methyl}) \text{R2}$ (24)+ $\delta(\text{HCC}) \text{R1}$ (16)
1158	1178	1175	$\nu(\text{CC}) \text{R2}$ (12)+ $\nu(\text{C-C}_\text{methine})$ (12)
1127	1143	1142	$\nu(\text{CC}) \text{R1}$ (25)+ $\rho(\text{C}-\text{H}) \text{R1}$ (19)+ $\rho(\text{C}-\text{H}) \text{R1}$ (24)
	1110	1109	$\nu(\text{CC}) \text{R2}$ (17)+ $\rho(\text{C}-\text{H}) \text{R2}$ (27)+ $\rho(\text{C}-\text{H}) \text{R2}$ (30)
1097	1101	1101	$\nu(\text{CC}_\text{methyl}) \text{R1}$ (12)+ $\delta(\text{HCC}) \text{R1}$ (19)
	1073	1069	$\nu(\text{CC}) \text{R2}$ (16)+ $\nu(\text{CC}) \text{R2}$ (18)+ $\nu(\text{CN})$ (15)+ $\rho(\text{CH}) \text{R2}$ (14)+ $\rho(\text{CH}) \text{R2}$ (24)
1020	1034	1039	$\tau(\text{CCC}_\text{methyl}\text{H})$ (29)+ $\tau(\text{CCC}_\text{methyl}\text{H})$ (11)+ $\tau(\text{CCC}_\text{methyl}\text{H})$ (11)
1009	1011	1014	$\tau(\text{CCC}_\text{methyl}\text{H})$ (28)+ $\tau(\text{CCC}_\text{methyl}\text{H})$ (18)
1001	995	996	$\tau(\text{CCC}_\text{methyl}\text{H})$ (20)+ $\tau(\text{CCC}_\text{methyl}\text{H})$ (22)
980	984	984	$\delta(\text{CCC}) \text{R1}$ (11)+ $\tau(\text{HCCC})$ (19)+ $\tau(\text{CCC}_\text{methyl}\text{H})$ (21)
	967	974	$\tau(\text{HCNC})$ (67)
951	956	970	$\tau(\text{HCCC}) \text{R2}$ (45)+ $\tau(\text{HCCC}) \text{R2}$ (24)+ $\tau(\text{CCCC}) \text{R2}$ (15)
942	943	947	$\delta(\text{CCC}) \text{R1}$ (10)
	934	939	$\tau(\text{HCCC}) \text{R1}$ (29)+ $\tau(\text{HCCC}) \text{R1}$ (29)+ $\tau(\text{CCCC}) \text{R1}$ (10)
924	929	927	$\nu(\text{C}-\text{NO}_2)$ (10)+ $\delta(\text{CCC}) \text{R2}$ (14)+ $\delta(\text{CCC}) \text{R2}$ (11)
906	899	913	$\gamma(\text{HCC}) \text{R2}$ (71)
882	883	894	$\tau(\text{HOCC}) \text{R2}$ (87)
	858	868	$\tau((\text{HCCC}) \text{R1})$ (58)+ $\tau(\text{CCCC}) \text{R1}$ (12)
842	829	836	$\delta(\text{ONO})$ (34)+ $\tau(\text{HCCC}) \text{R1}$ (10)
830	822	827	$\tau(\text{HCCC}) \text{R2}$ (40)+ $\tau(\text{HCCC}) \text{R2}$ (28)+ $\gamma(\text{OCCC}) \text{R2}$ (11)
	811	818	$\tau(\text{HCCC}) \text{R1}$ (35)+ $\tau(\text{HCCC}) \text{R1}$ (40)
793	780	779	$\delta(\text{CCC}) \text{R2}$ (21)+ $\delta(\text{CC}=\text{N})$ (10)
776	763	761	$\delta(\text{CCC}) \text{R2}$ (10)+ $\delta(\text{CCC}) \text{R2}$ (12)
752	733	756	$\nu(\text{CC}_\text{methyl}) \text{R1}$ (12)+ $\delta(\text{CCC}) \text{R1}$ (13)+ $\delta(\text{CCC}) \text{R1}$ (13)+ $\delta(\text{CCC}) \text{R1}$ (13)+ $\delta(\text{CCC}) \text{R1}$ (21)
725	711	732	$\tau(\text{HCCC}) \text{R2}$ (15)+ $\gamma(\text{OCCC}) \text{R2}$ (26)+ $\tau(\text{CCCC}) \text{R2}$ (10)
706	704	728	$\gamma(\text{OCON})$ (80)
672	697	708	$\tau(\text{CCCC}) \text{R1}$ (15)+ $\tau(\text{CCCC}) \text{R1}$ (14)
638	661	660	$\delta(\text{CCC}) \text{R1}$ (10)
	630	630	$\delta(\text{CCC}) \text{R2}$ (15)
587	583	588	$\gamma(\text{NCCC}) \text{R1}$ (23)+ $\gamma(\text{CCCC}) \text{R1}$ (11)
570	554	555	$\nu(\text{CC}_\text{methyl}) \text{R1}$ (11)+ $\delta(\text{CCC}) \text{R1}$ (14)
546	538	540	$\delta(\text{ONC}) \text{R2}$ (27)+ $\delta(\text{CCC}) \text{R1}$ (12)
531	522	533	$\tau(\text{CCCC}) \text{R2}$ (10)+ $\tau(\text{CCCC}) \text{R2}$ (12)
501	501	504	$\delta(\text{NCC}) \text{R1}$ (19)+ $\delta(\text{CCC}_\text{methyl}) \text{R1}$ (11)
476	492	491	$\delta(\text{CCC}) \text{R1}$ (13)

(continued on next page)

Table 1 (continued)

Experimental	GTO	STO	Assignment (%PED ^a)
464	454	461	$\tau(\text{CCCC}) \text{R}2$ (28) + $\tau(\text{CCCC}) \text{R}1$ (10) + $\tau(\text{OCCC})$ (13)
449	437	442	$\tau(\text{CCCC}) \text{R}1$ (24) + $\gamma(\text{CCCC}_{\text{methyl}}) \text{R}1$ (16)
433	431	431	$\delta(\text{CC}) \text{R}2$ (12) + $\delta(\text{ONC}) \text{R}2$ (10) + $\delta(\text{OCC}) \text{R}2$ (38)
417	399	398	$\delta(\text{CCC}_{\text{methine}}) \text{R}2$ (14) + $\delta(\text{CCC}_{\text{methyl}}) \text{R}1$ (13) + $\delta(\text{OCC})$ (38)
404	353	356	$\tau(\text{CC}=\text{NC})$ (10) + $\gamma(\text{CCCC}_{\text{methyl}}) \text{R}1$ (19)
	348	347	$\nu(\text{C}-\text{NO}_2)$ (28) + $\delta(\text{CCC}) \text{R}2$ (15)
	330	332	$\tau(\text{CCCC}_{\text{methine}})$ (15) + $\tau(\text{CCCC}) \text{R}2$ (19) + $\gamma(\text{OCCC})$ (13)
	293	297	$\delta(\text{CC}) \text{R}1$ (14) + $\delta(\text{CCC}_{\text{methyl}})$ (39) + $\delta(\text{CCC}_{\text{methyl}})$ (32)
	282	281	$\delta(\text{ONC})$ (10) + $\delta(\text{CCC}_{\text{methine}})$ (14) + $\delta(\text{NCC}) \text{R}1$ (10) + $\delta(\text{ONCC})$ (11)
	257	259	$\tau(\text{CCC}=\text{N}) \text{R}2$ (24) + $\gamma(\text{NCCC}) \text{R}2$ (33)
	230	231	$\delta(\text{NCC}) \text{R}2$ (10) + $\tau(\text{CCCC}) \text{R}1$ (11) + $\tau(\text{CCC}=\text{N}) \text{R}2$ (11) + $\gamma(\text{CCCC}_{\text{methyl}})$ (11) + $\gamma(\text{CCCC}_{\text{methyl}})$ (19)
184	183		$\nu(\text{CC}_{\text{methine}}) \text{R}2$ (11) + $\nu(\text{N}=\text{C}) \text{R}1$ (11) + $\delta(\text{CC}=\text{N}) \text{R}2$ (17) + $\delta(\text{ONCC})$ (22)
180	180		$\tau(\text{CCCC}) \text{R}1$ (10) + $\tau(\text{CCCC}) \text{R}1$ (20) + $\tau(\text{CCCC}_{\text{methyl}})$ (11)
159	168		$\tau(\text{CCC}_{\text{methylH}})$ (11) + $\tau(\text{CCC}_{\text{methylH}})$ (10)
152	154		$\delta(\text{NCC}) \text{R}1$ (12) + $\tau(\text{CCC}_{\text{methylH}})$ (10)
127	130		$\tau(\text{CCC}_{\text{methylH}})$ (18) + $\tau(\text{CCC}_{\text{methylH}})$ (19) + $\tau(\text{CCC}_{\text{methylH}})$ (11) + $\tau(\text{CCC}_{\text{methylH}})$ (14) + $\tau(\text{CCC}_{\text{methylH}})$ (13)
118	119		$\tau(\text{CCCC}) \text{R}2$ (26) + $\tau(\text{CCCC}) \text{R}1$ (13) + $\gamma(\text{NCCC}) \text{R}2$ (11)
106	105		$\tau(\text{CCCC}) \text{R}2$ (15) + $\gamma(\text{NCCC}) \text{R}2$ (19)
56	60		$\tau(\text{ONCC})$ (67) + $\tau(\text{CC}=\text{NC})$ (14)
45	43		$\delta(\text{CNC}) \text{R}2$ (38) + $\delta(\text{CCC}_{\text{methine}}) \text{R}2$ (10) + $\delta(\text{CC}=\text{N}) \text{R}2$ (10) + $\delta(\text{NCC}) \text{R}1$ (10)
35	37		$\tau(\text{ONCC})$ (19) + $\tau(\text{CCCC}_{\text{methine}}) \text{R}2$ (24) + $\tau(\text{CC}=\text{NC})$ (30) + $\gamma(\text{NCCC}) \text{R}1$ (10)
25	23		$\tau(\text{C}=\text{NCC}) \text{R}1$ (62) + $\tau(\text{CCC}=\text{N}) \text{R}2$ (20)

ν , stretching; δ , in-plane bending; γ , out-of-plane bending; τ , torsion; α , scissoring; ρ , rocking; s, symmetric; as, asymmetric. Abbreviations: R2, C1–C6; R1, C8–C13 phenyl ring.

^a Potential energy distribution were calculated with respect to GTO results.

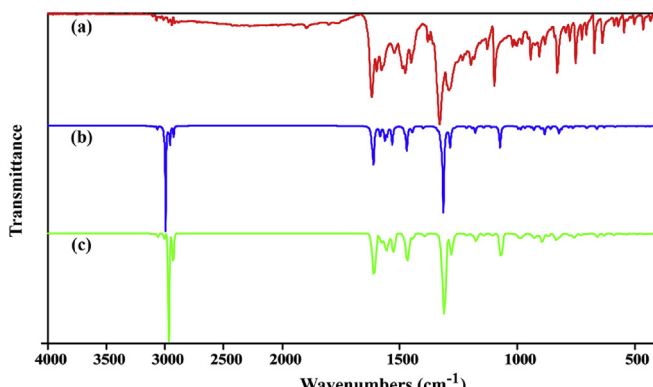


Fig. 6. The experimental (a), GTO (b) and STO (c) infrared spectra of the compound.

with the increasing solvent polarity. As suggested in section 3.2., the proton transfer can occur easily in the high polarity solvent.

3.5. ^1H and ^{13}C NMR spectroscopy

The ^1H and ^{13}C NMR spectra in the DMSO solvent of the compound are shown in Fig. S2. Due to strong intramolecular O–H···N type hydrogen bond, chemical shift of the hydroxyl proton is located at 14.73 ppm. The peak at 9.19 ppm represents the resonance of imino proton.

The peaks of H6 and H4 protons were shifted to down field region by nitro group which is a strong electron withdrawing group. The other aromatic hydrogens are located between 7.32 and 7.09 ppm while the methyl protons give peaks at 2.50 and 2.28 ppm. In the ^{13}C NMR spectrum, due to the downfield effect of electronegative atoms, the phenolic carbon (C2) peak was observed at 168.2 ppm and the imine carbon (C7) peak was appeared at 161.1 ppm. Peaks of the nitrogen single bonded aromatic C8 and C5 carbon atoms appear at 143.8 and 139.2 ppm. Chemical shifts of the other aromatic carbons are located at 130–110 ppm region. The methyl carbons give peaks at about ~20 ppm.

3.6. Non-linear optical properties

Schiff bases and their metal complexes can show non-linear optical (NLO) response and thus they can be used in optical communication and computing technologies [63–66]. In the Schiff bases, NLO properties can be caused by the delocalization of π electrons and the enol/keto tautomerism. The NLO properties may increase depending on the conjugation and donor/acceptor groups of the molecule [67]. The title compound, has the delocalized π electron system with strong electron-withdrawing substituents nitro (NO_2) group, which enhance the delocalization of conjugated molecules. As pointed in previous studies [68,69], the polar molecules having non-zero dipole moment can show microscopic NLO behavior, even if they crystallized in the centrosymmetric space group. In order to find out the NLO properties of the title molecule, the dipole moment, polarizability and the first order hyperpolarizability were obtained at the DFT/B3LYP/6-311++G (d,p) level of theory. Calculated values of these are 6.357 Debye, 35.618 \AA^3 and $29.301 \times 10^{-30} \text{ cm}^5/\text{esu}$, respectively. *p*-nitroaniline (μ , α and β values are 7.146 Debye, 12.721 \AA^3 and $11.463 \times 10^{-30} \text{ cm}^5/\text{esu}$ obtained by B3LYP/6-31G(d) method), is a common reference material to compare NLO properties of a conjugated organic compound [70]. Calculated polarizability and first order hyperpolarizability values of the title compound are nearly three times greater than those of *p*-nitroaniline. Therefore, based on these results, one can expect that the studied compound can show good NLO activity.

3.7. NBO analysis

NBO analysis is a useful method and emphasizes the role of intra- and inter-molecular interactions, interaction among bonds, conjugative interactions in the molecular systems. These interactions can be quantitatively described in terms of NBO approach which is expressed by means of second-order perturbation interaction energy, $E^{(2)}$ [71]. Delocalization of electron density between occupied Lewis type (CR, σ , π or LP) NBOs and formally unoccupied (antibond or Rydberg) non-Lewis NBO corresponds to a stabilizing donor–acceptor interaction [72]. NBO analysis of the

molecule has been performed by using Gaussian NBO Version 3.1 program in the Gaussian 09W package at the DFT/B3LYP/6-311++G (d,p) level. The results of second-order perturbation theory analysis of the Kohn-Sham Matrix are presented in Table S5. In the table, stabilization energies were selected as larger than 3 kcal/mol⁻¹.

Interactions of π -electrons in the rings give the greatest intramolecular hyperconjugative interaction energy and their values are C1–C6 → C7–N1 (22.97 kcal/mol), C8–C13 → C11–C12 (19.86 kcal/mol), C9–C10 → C8–C13 (21.2 kcal/mol), C11–C12 → C8–C13 (21.31 kcal/mol) and C9–C10 (20.83 kcal/mol). Hyperconjugative interactions of the $\sigma \rightarrow \sigma^*$ transitions are weak and their energies less than 5 kcal/mol.

LP (3)(O3) → π^* (N2–O2) interaction gives a strong stabilization to the system by 149.55 kcal/mol. In addition, the other important interaction of the LP (1)(C5) → π^* (N2–O2) has the enormous stabilization energy of 370.68 kcal/mol. Also, intramolecular hydrogen bond energy can be calculated by evaluating lone pair N1 to the σ -type antibonding O1–H1 interaction which the resulting stabilization energy is 5.16 kcal/mol.

The NBO analysis also describes the bonding concepts (the bond occupancies, percentage electron density over bonded atoms, the natural atomic hybrids (sp^x)). As shown in Table S5, the bonding orbital for C1–C2 with 1.97250 electrons has 51.05% C1 character in a $sp^{2.05}$ hybrid and has 48.95% C2 character in a $sp^{1.72}$ hybrid orbital. The bonding orbital for C7–N1 with 1.91547 electrons has 38.74% C7 character in a $sp^{99.99}$ hybrid and has 61.26% N1 character in a $sp^{99.9}$ hybrid orbital. The bonding orbital for N2–O2 with 1.98628 electrons has 39.26% N2 character in a $sp^{1.00}$ hybrid and has 60.74% O2 character in a $sp^{1.00}$ hybrid orbital.

4. Conclusion

The single crystal XRD and the geometry optimization studies of (E)-2-((3,4-dimethylphenylimino)methyl)-4-nitrophenol compound show that both the GTO and STO type calculations yield a good match for experimental and computational structure. The XRD and FT-IR studies clearly revealed the enol structure is more dominant than the keto form in solid state. From the results of the UV–Vis. spectroscopy and the potential energy surface scan calculations, we can conclude that the enol/keto ratio decreases with the increasing solvent polarity. When considering the optimized geometry section and the infrared section, there is no significant difference between the two basis sets. Calculated polarizability and first hyperpolarizability values indicate that the title compound can be used as a good non-linear optical material.

Acknowledgements

Authors thank to Prof. Orhan Büyükgüngör for helping in XRD data collection. This study supported by Ondokuz Mayıs University (PYO.FEN.1901.10) and Giresun University (FEN-BAP-A-250414-75).

Appendix A. Supplementary data

Supplementary data related to this article can be found at <http://dx.doi.org/10.1016/j.molstruc.2016.07.117>.

References

- [1] H. Tanak, Molecular structure, spectroscopic (FT-IR and UV-Vis) and DFT quantum-chemical studies on 2-[(2,4-Dimethylphenyl)iminomethyl]-6-methylphenol, *Mol. Phys.* 112 (2014) 1553–1565.
- [2] Ç. Albayrak, G. Kaştaş, M. Odabaşoğlu, O. Büyükgüngör, Existence of a resonance hybrid structure as a result of proton tautomerism in (\pm)-(E)-4-Bromo-2-[(2,3-dihydroxypropylimino) methyl]phenol racemate, *Spectrochim. Acta Part A Mol. Biomol. Spectrosc.* 120 (2014) 201–207.
- [3] Ç. Albayrak, B. Koşar, S. Demir, M. Odabaşoğlu, O. Büyükgüngör, Synthesis, spectroscopic, molecular and computational structure characterizations of (E)-2-ethoxy-6-[(phenylimino)methyl]phenol, *J. Mol. Struct.* 963 (2010) 211–218.
- [4] Z. Demircioğlu, Ç. Albayrak, O. Büyükgüngör, Theoretical and experimental investigation of (E)-2-[(3,4-dimethylphenyl) imino)methyl]-3-methoxyphenol: enol-keto tautomerism, spectroscopic properties, NLO, NBO and NPA analysis, *J. Mol. Struct.* 1065–1066 (2014) 210–222.
- [5] B. Kosar, C. Albayrak, Spectroscopic investigations and quantum chemical computational study of (E)-4-methoxy-2-[(p-tolylimino)methyl]phenol, *Spectrochim. Acta Part A Mol. Biomol. Spectrosc.* 78 (2011) 160–167.
- [6] K. Ogawa, J. Harada, T. Fujiwara, S. Yoshida, Thermochromism of salicylideneanilines in solution: aggregation-controlled proton tautomerization, *J. Phys. Chem. A* 105 (2001) 3425–3427.
- [7] D. Guha, A. Mandal, A. Koll, A. Filarowski, S. Mukherjee, Proton transfer reaction of a new orthohydroxy Schiff base in protic solvents at room temperature, *Spectrochim. Acta - Part A Mol. Biomol. Spectrosc.* 56 (2000) 2669–2677.
- [8] M.Z. Zgierski, A. Grabowska, Theoretical approach to photochromism of aromatic Schiff bases: a minimal chromophore salicylidene methylamine, *J. Chem. Phys.* 113 (2000) 7845–7852.
- [9] M.E. Kletskii, A.A. Milov, A.V. Metelitsa, M.I. Knyazhansky, Role of structural flexibility in the fluorescence and photochromism of salicylideneaniline: the general scheme of the phototransformations, *J. Photochem. Photobiol. A* 110 (1997) 267–270.
- [10] Ü. Ceylan, M. Durgun, H. Türkmen, S.P. Yalçın, A. Kılıç, N. Özdemir, Theoretical and experimental investigation of 4-[(2-hydroxy-3-methylbenzylidene) amino] benzenesulfonamide: structural and spectroscopic properties, NBO, NLO and NPA analysis, *J. Mol. Struct.* 1089 (2015) 222–232.
- [11] T. Maki, H. Hashimoto, Vat dyes of acenaphthene series. IV. Condensation of perylenetetracarboxylic acid anhydride with o-phenylenediamine, *Bull. Chem. Soc. Jpn.* 25 (1952) 411–413.
- [12] S. Papic, N. Koprivancic, Z. Grabaric, D. Parac-Osterman, Metal complex dyes of nickel with Schiff bases, *Dye. Pigment* 25 (1994) 229–240.
- [13] K. Amimoto, T. Kawato, Photochromism of organic compounds in the crystal state, *J. Photochem. Photobiol. C Photochem. Rev.* 6 (2005) 207–226.
- [14] B. Jarzabek, B. Kaczmarczyk, D. Sek, Characteristic and spectroscopic properties of the Schiff-base model compounds, *Spectrochim. Acta - Part A Mol. Biomol. Spectrosc.* 74 (2009) 949–954.
- [15] V. Ambike, S. Adsule, F. Ahmed, Z. Wang, Z. Afrasiabi, E. Sinn, F. Sarkar, S. Padhye, Copper conjugates of nimesulide Schiff bases targeting VEGF, COX and Bcl-2 in pancreatic cancer cells, *J. Inorg. Biochem.* 101 (2007) 1517–1524.
- [16] S. Zolezzi, E. Spodine, A. Decinti, Electrochemical studies of copper(II) complexes with Schiff-base ligands, *Polyhedron* 21 (2002) 55–59.
- [17] M. Singh, Transferrin as a targeting ligand for liposomes and anticancer drugs, *Curr. Pharm. Des.* 5 (1999) 443–451.
- [18] I. Moustakali-Mavridis, E. Hadjoudis, A. Mavridis, Crystal and molecular structure of some thermochromic Schiff bases, *Acta Crystallogr. Sect. B Struct. Crystallogr. Cryst. Chem.* 34 (1978) 3709–3715.
- [19] G. Pistoris, D. Geigou, E. Hadjoudis, Effect of cyclodextrin complexation on thermochromic Schiff bases, *J. Photochem. Photobiol. A Chem.* 93 (1996) 179–184.
- [20] A. Lapworth, A.C.O. Hann, CXLIX.—The mutarotation of camphorquinonehydrazone and mechanism of simple desmotropic change, *J. Chem. Soc. Trans.* 81 (1902) 1508–1519.
- [21] A. Özak, Ç. Albayrak, M. Odabaşoğlu, O. Büyükgüngör, Three (E)-2-[(bromophenyl)iminomethyl]-4-methoxyphenols, *Acta Crystallogr. Sect. C Cryst. Struct. Commun.* 63 (2007) o177–o180.
- [22] H. Tanak, F. Erşahin, E. Ağar, O. Büyükgüngör, M. Yavuz, Crystal structure of N-2-Methoxyphenyl-2-oxo-5-nitro-1-benzylidene-methylamine, *Anal. Sci. X-Ray Struct. Anal. Online* 24 (2008) x237–x238.
- [23] A. Blagus, D. Činčić, T. Fršić, B. Kaitner, V. Stilinović, Schiff bases derived from hydroxaryl aldehydes: molecular and crystal structure, tautomerism, quinoid effect, coordination compounds, *Maced. J. Chem. Chem. Eng.* 29 (2010) 117–138.
- [24] G.M. Sheldrick, A short history of SHELX, *Acta Crystallogr. Sect. A Found. Crystallogr.* 64 (2007) 112–122.
- [25] L.J. Farrugia, WinGX and ORTEP for Windows: an update, *J. Appl. Crystallogr.* 45 (2012) 849–854.
- [26] L.J. Farrugia, ORTEP-3 for Windows – a version of ORTEP-III with a graphical user interface (GUI), *J. Appl. Crystallogr.* 30 (1997) 565.
- [27] A.L. Spek, Single-crystal structure validation with the program PLATON, *J. Appl. Crystallogr.* 36 (2003) 7–13.
- [28] M.J. Frisch, G.W. Trucks, H.B. Schlegel, G.E. Scuseria, M.A. Robb, J.R. Cheeseman, G. Scalmani, V. Barone, B. Mennucci, G.A. Petersson, H. Nakatsuji, M. Caricato, X. Li, H.P. Hratchian, A.F. Izmaylov, J. Bloino, G. Zheng, J.L. Sonnenberg, M. Hada, M. Ehara, K. Toyota, R. Fukuda, J. Hasegawa, M. Ishida, T. Nakajima, Y. Honda, O. Kitao, H. Nakai, T. Vreven, J.A. Montgomery Jr., J.E. Peralta, F. Ogliaro, M. Bearpark, J.J. Heyd, E. Brothers, K.N. Kudin, V.N. Staroverov, R. Kobayashi, J. Normand, K. Raghavachari, A. Rendell, J.C. Burant, S.S. Iyengar, J. Tomasi, M. Cossi, N. Rega, J.M. Millam, M. Klene, J.E. Knox, J.B. Cross, V. Bakken, C. Adamo, J. Jaramillo, R. Gomperts, R.E. Stratmann, O. Yazyev, A.J. Austin, R. Cammi, C. Pomelli, J.W. Ochterski, R.L. Martin, K. Morokuma, V.G. Zakrzewski, G.A. Voth, P. Salvador,

- J.J. Dannenberg, S. Dapprich, A.D. Daniels, Ö. Farkas, J.B. Foresman, J.V. Ortiz, J. Cioslowski, D.J. Fox, Gaussian 09, Revision E.01, Gaussian, Inc., Wallingford CT, 2009.
- [29] A.D. Becke, Density-functional thermochemistry.III. The role of exact exchange, *J. Chem. Phys.* 98 (1993) 5648.
- [30] C.Y. Peng, P.Y. Ayala, H.B. Schlegel, M.J. Frisch, Using redundant internal coordinates to optimize equilibrium geometries and transition states, *J. Comput. Chem.* 17 (1996) 49–56.
- [31] J.P. Merrick, D. Moran, L. Radom, An evaluation of harmonic vibrational frequency scale factors, *J. Phys. Chem. A* 111 (2007) 11683–11700.
- [32] A. Akbari, Z. Alinia, Synthesis, characterization, and DFT calculation of a Pd(II) Schiff base complex, *Turk. J. Chem.* 37 (2013) 867–878.
- [33] M.H. Jamróz, Vibrational Energy Distribution Analysis (VEDA) 4, 2015. Warsaw.
- [34] E. Runge, E.K.U. Gross, Density-functional theory for time-dependent systems, *Phys. Rev. Lett.* 52 (1984) 997–1000.
- [35] R.E. Stratmann, G.E. Scuseria, M.J. Frisch, An efficient implementation of time-dependent density-functional theory for the calculation of excitation energies of large molecules, *J. Chem. Phys.* 109 (1998) 8218–8224.
- [36] R. Bauernschmitt, R. Ahlrichs, Treatment of electronic excitations within the adiabatic approximation of time dependent density functional theory, *Chem. Phys. Lett.* 256 (1996) 454–464.
- [37] M.E. Casida, C. Jamorski, K.C. Casida, D.R. Salahub, Molecular excitation energies to high-lying bound states from time-dependent density-functional response theory: characterization and correction of the time-dependent local density approximation ionization threshold Mark, *J. Chem. Phys.* 108 (1998) 4439.
- [38] J. Tomasi, B. Mennucci, R. Cammi, Quantum mechanical continuum solvation models, *Chem. Rev.* 105 (2005) 2999–3093.
- [39] E. Cancès, B. Mennucci, J. Tomasi, A new integral equation formalism for the polarizable continuum model: theoretical background and applications to isotropic and anisotropic dielectrics, *J. Chem. Phys.* 107 (1997) 3032.
- [40] F.M. Bickelhaupt, Chemistry with ADF, *J. Comput. Chem.* 22 (2001) 931–967.
- [41] C. Fonseca Guerra, J.G. Snijders, G. Te Velde, E.J. Baerends, Towards an order- N DFT method, *Theory Chem. Accounts Theory Comput. Model. Theoretica Chim. Acta* 99 (1998) 391–403.
- [42] ADF2009.01, SCM, Theoretical Chemistry, Vrije Universiteit, Amsterdam, The Netherlands, <http://www.scm.com>.
- [43] A. Özak, Ç. Albayrak, M. Odabaşoğlu, O. Büyükgüngör, Crystallographic and conformational analysis of [(E)-2-[(3-Chlorophenylimino)methyl]-4-methoxyphenol], *J. Chem. Crystallogr.* 39 (2008) 353–357.
- [44] Ç. Albayrak, G. Kaşaş, M. Odabaşoğlu, R. Frank, Probing the compound (E)-5-(diethylamino)-2-[(4-methylphenylimino)methyl] phenol mainly from the point of tautomerism in solvent media and the solid state by experimental and computational methods, *Spectrochim. Acta - Part A Mol. Biomol. Spectrosc.* 81 (2011) 72–78.
- [45] I. Moustakali-Mavridis, E. Hadjoudis, A. Mavridis, Crystal and molecular structure of some thermochromic Schiff bases, *Acta Crystallogr. Sect. B Struct. Crystallogr. Cryst. Chem.* 34 (1978) 3709–3715.
- [46] H. Tanak, Crystal structure, spectroscopy, and quantum chemical studies of (E)-2-[(2-Chlorophenyl)iminomethyl]-4-trifluoromethoxyphenol, *J. Phys. Chem. A* 115 (2011) 13865–13876.
- [47] B. Koşar, C. Albayrak, C.C. Ersanlı, M. Odabaşoğlu, O. Büyükgüngör, Molecular structure, spectroscopic investigations, second-order nonlinear optical properties and intramolecular proton transfer of (E)-5-(diethylamino)-2-[(4-propylphenylimino)methyl]phenol: a combined experimental and theoretical study, *Spectrochim. Acta. A. Mol. Biomol. Spectrosc.* 93 (2012) 1–9.
- [48] A. Bondi, van der Waals Volumes and Radii, *J. Phys. Chem.* 68 (1964) 441–451.
- [49] J. Kruszewski, T.M. Krygowski, Definition of aromaticity basing on the harmonic oscillator model, *Tetrahedron Lett.* 13 (1972) 3839–3842.
- [50] T.M. Krygowski, Crystallographic studies of inter- and intramolecular interactions reflected in aromatic character of Pi-electron systems, *J. Chem. Inf. Model.* 33 (1993) 70–78.
- [51] A. Filarowski, A. Koll, T. Glowik, Low barrier hydrogen bonds in sterically modified Schiff bases, *J. Chem. Soc. Perkin Trans. 2* (2002) 835–842.
- [52] A. Filarowski, A. Kochel, M. Kluba, F.S. Kamounah, Structural and aromatic aspects of tautomer equilibrium in hydroxy aryl Schiff bases, *J. Phys. Org. Chem.* 21 (2008) 939–944.
- [53] H. Karabiyik, H. Petek, N.O. Iskeleli, Ç. Albayrak, Structural and aromatic aspects for tautomerism of (Z)-6-((4-bromophenylamino)methylene)-2,3-dihydroxycyclohexa-2,4-dienone, *Struct. Chem.* 20 (2009) 1055–1065.
- [54] Ç. Albayrak, G. Kaşaş, M. Odabaşoğlu, R. Frank, The prototropic tautomerism and substituent effect through strong electron-withdrawing group in (E)-5-(diethylamino)-2-(3-nitrophenylimino)methyl phenol, *Spectrochim. Acta - Part A Mol. Biomol. Spectrosc.* 114 (2013) 205–213.
- [55] B. Stuart, *Infrared Spectroscopy: Fundamentals and Applications*, John Wiley & Sons, Inc., England, 2004.
- [56] R.M. Silverstein, F.X. Webster, D. Kiemle, D.L. Bryce, *Spectrometric Identification of Organic Compounds*, John Wiley & Sons, Inc., England, 1991.
- [57] E.E. Porchelvi, S. Muthu, Vibrational spectra, molecular structure, natural bond orbital, first order hyperpolarizability, thermodynamic analysis and normal coordinate analysis of Salicylaldehyde p-methylphenylthiosemicarbazone by density functional method, *Spectrochim. Acta - Part A Mol. Biomol. Spectrosc.* 134 (2015) 453–464.
- [58] M.C.B. Wojtkowiak, *Spectrochimie moléculaire*, Mater. Chem. 2 (1977) 109–110.
- [59] H. Barańska, A. Labudzinska, J. Terpinski, *Laser Raman Spectroscopy: Analytical Applications*, PWN Polish Scientific Publishers/Ellis Harwood Limited Publishers, 1987.
- [60] N.M. O'boyle, A.L. Tenderholt, K.M. Langner, cclib: a library for package-independent computational chemistry algorithms, *J. Comput. Chem.* 29 (2008) 839–845.
- [61] N. Özdemir, S. Dayan, O. Dayan, M. Dinçer, N.Ö. Kalaycıoğlu, Experimental and molecular modeling investigation of (E)-N-(2-[(2-hydroxybenzylidene)amino]phenyl)benzenesulfonamide, *Mol. Phys.* 111 (2012) 707–723.
- [62] G. Kaşaş, Investigating the prototropic tautomerism in (E)-2-[(4-fluorophenyl) iminomethyl]-5-methoxyphenol compound for solid state and solvent media by experimental and quantum computational tools, *J. Mol. Struct.* 1017 (2012) 38–44.
- [63] P.V. Kolinski, New materials and their characterization for photonic device applications, *Opt. Eng.* 31 (1992) 1676–1684.
- [64] N. Chand, Nonlinear optical materials, *chem. Mater* 4 (1992) 930.
- [65] M. Sliwa, S. Létard, I. Malfant, M. Nierlich, P.G. Lacroix, T. Asahi, H. Masuhara, P. Yu, K. Nakatani, Design, synthesis, structural and nonlinear optical properties of photochromic crystals: toward reversible molecular switches, *Chem. Mater.* 17 (2005) 4727–4735.
- [66] S. Di Bella, I. Fragalà, I. Ledoux, M.A. Diaz-Garcia, T.J. Marks, Synthesis, characterization, optical spectroscopic, electronic structure, and second-order nonlinear optical (NLO) properties of a novel class of Donor–Acceptor bis(salicylaldiminato)nickel(II) Schiff base NLO chromophores, *J. Am. Chem. Soc.* 119 (1997) 9550–9557.
- [67] K.S. Thanthiriwatte, K. Nalin de Silva, Non-linear optical properties of novel fluorenyl derivatives—ab initio quantum chemical calculations, *J. Mol. Struct. Theochem.* 617 (2002) 169–175.
- [68] A. Elmali, A. Karakaş, H. Ünver, Nonlinear optical properties of bis((p-bromophenyl-salicylaldiminato)chloroiron(III)) and its ligand N-(4-bromo)salicylaldimine, *Chem. Phys.* 309 (2005) 251–257.
- [69] S. Suresh, A. Ramanand, D. Jayaraman, P. Mani, Review on theoretical aspect of nonlinear optics, *Rev. Adv. Mater. Sci.* 30 (2012) 175–183.
- [70] M. Yavuz, H. Tanak, Density functional modelling studies on N-2-Methoxyphenyl-2-oxo-5-nitro-1-benzylidenemethylamine, *J. Mol. Struct. Theochem.* 961 (2010) 9–16.
- [71] J.P. Foster, F. Weinhold, Natural hybrid orbitals, *J. Am. Chem. Soc.* 102 (1980) 7211–7218.
- [72] H. Tanak, M. Yavuz, Density functional computational studies on (E)-2-[(2-Hydroxy-5-nitrophenyl)-iminomethyl]-4-nitrophenolate, *J. Mol. Model.* 16 (2010) 235–241.